Post-mortem analysis of the deposit layers on the lower divertor after the 2023 high particle fluence campaign of WEST

C. Martin, M. Diez, E. Bernard, M. Cabié, A. Campos, C. Pardanaud, G. Giacometti, A. Gallo, J. Gaspar, Y. Corre

Nuclear Materials and Energy 41 (2024) 101764

Contents lists available at ScienceDirect

Nuclear Materials and Energy

journal homepage: www.elsevier.com/locate/nme

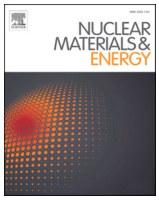

Post-mortem analysis of the deposit layers on the lower divertor after the 2023 high particle fluence campaign of WEST

C. Martin [a,*], M. Diez [b], E. Bernard [b], M. Cabié [c], A. Campos [c], C. Pardanaud [a], G. Giacometti [a], A. Gallo [b], J. Gaspar [d], Y. Corre [b], E.Tsitrone [b], the WEST team [1]

[a] Aix Marseille Univ, CNRS, PIIM, Marseille, France
[b] CEA, IRFM, F-13108 St Paul lez Durance, France
[c] Aix Marseille Univ, CNRS, CP2M, Marseille, France
[d] Aix Marseille Univ, CNRS, IUSTI, Marseille, France

A B S T R A C T

We analysed deposits collected on the lower divertor of WEST after the first high fluence campaign performed in 2023. Deposits were collected on the high field side (thick deposition area) of 2 ITER-grade plasma facing units (PFUs), located on different toroidal positions. Using focused ion beam cross sectioning, the deposits were found to be very thick (12–55 μm). A significant difference was observed in the toroidal direction with thicker deposits for the PFU located at the maximal heat load in the inner side, showing a deposition pattern due to the toroidal magnetic field modulation. Deposits present a complex layer-by-layer structure with dense layers, some melted parts and porosities within the layers. The deposition is mainly composed of tungsten with oxygen, boron, carbon and traces of nitrogen whose composition vary along the radial direction. We identified W-rich deposits in the high plasma flux area near the inner strike point and deposits rich in O, B, C and N in the low plasma flux area further away from this strike point. W dense layers of about 5 up to 40 μm thick in the thick deposit area near the strike point were attributed to the high fluence campaign. Pure boron layers resulting from wall conditioning and processed by plasma wall interactions were also observed.

Introduction

Understanding the material migration and subsequent deposited layers in a fully metallic environment is one of the key issue for next step fusion devices as ITER. During its second phase of operation, the lower divertor of the WEST tokamak was fully equipped with actively cooled ITER-grade plasma facing units (PFUs) made of 35 tungsten monoblocks (MBs) [1]. The PFUs are based on the ITER divertor technology (fixation on the copper tube of the cooling loop [2]) and on the shaping ITER baseline (bevel 1° and 0.5 mm height [3]). In WEST the temperature of the water cooling loop is 70 °C and the bevel is oriented to protect the leading edge avoiding the risk of cracks as it has been observed during the first phase of WEST [4]. With the aim of testing the divertor under real tokamak conditions prior to ITER operation, a first high particle fluence campaign (second part of C7 campaign) has been performed in WEST by repeating a large number of long discharges (60–70 s of pulse length) with an attached L-mode of D divertor plasma (Te≈25 eV). A cumulated plasma duration of 3 h was reached with a total fluence of about 5.10^{26} D.m^{-2} at the outer strike point (OSP) of the divertor corresponding to 2 shots in the pre-fusion plasma operation phase of ITER [5]. Mobilization of deposits has been identified as the cause of the appearance of unidentified flying object (UFO) entering the core plasma, which affecting the discharges by increasing the core density and the total radiated power. This leads to early plasma instabilities and an increase of the plasma disruptivity [6].

Deposition is mainly due to erosion, transport and redeposition during plasma exposure, but can also be influenced by wall conditioning procedures. Wall conditioning in WEST prior to plasma discharges consists of baking up to 170°C for water depletion, glow discharges cleaning and ends by glow discharge boronisation through a He carrier glow discharge with 85 %He + 15 %B_2D_6 [7]. Boronisation in WEST, which reduces the intrinsic impurity of oxygen, has been shown to improve operating conditions and has a lasting impact on disruptions [1]. The reduction in total radiation can be correlated with the decrease in oxygen content and the deposited B layer covering the W, both of which have the effect of reducing W sputtering. During the high fluence campaign dedicated to plasma wall interaction studies, no boronisation between each repetition of plasma discharges were performed.

With the aim to analyze the high fluence campaign effect on deposition, especially for the W and B species, we characterized the

* Corresponding author.
E-mail address: celine.martin@univ-amu.fr (C. Martin).
[1] http://west.cea.fr/WESTteam.

https://doi.org/10.1016/j.nme.2024.101764
Received 16 June 2024; Received in revised form 6 October 2024; Accepted 8 October 2024
Available online 11 October 2024

Table 1
Overview of the achievements of the WEST C5 to C7 campaigns. Number of plasma discharges, cumulated plasma duration, number of disruptions, total injected energy using both ion cyclotron resonance heating (ICRH) and lower hybrid current drive (LHCD) and number of boronisations.

	Nb plasmas	Cumulated time (s)	Nb disruptions	W total (GJ)	Boronisation
C5	655	4630	460	2.8	2
C6	47	295	21	0	1
C7 Part I	668	8796	327	13.4	1
C7 High fluence	445	10869	354	30.1	0

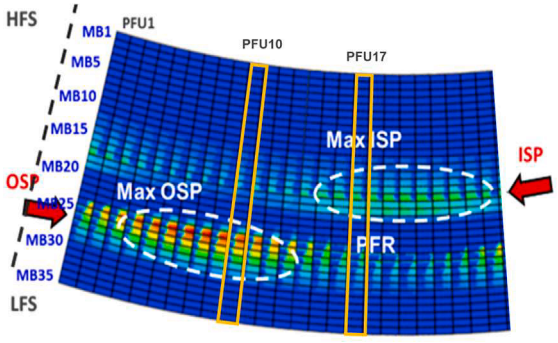

Fig. 1. Part of a sector (PFU1 to PFU25 over the 38 PFUs) of the WEST lower divertor showing the typical heat load on WEST divertor simulated by PFCflux code. The PFUs on which deposits have been collected are PFU10 located in the OSP max area and PFU17 located in the ISP max area (yellow frame).

morphology and composition of deposits on the inner side of the lower divertor, i.e. thick deposits of the high field side far scrape-off layer area. Finding clues about the structure and composition of the deposits that explain the formation of UFOs also motivates this work.

History, visual aspect and location of deposits

Two of the 38 ITER-grade PFUs located on one of the 12 modular sectors (sector Q3B) of the lower divertor were selected after the high-fluence campaign. They were installed in 2020 in the Q3B sector so they were both exposed to the C5 to C7 campaigns, with one boronisation systematically used before the plasma restart of each campaign, and one more carried out during C5. Table 1, give a short description of the C5 (Nov20-Jan21), C6 (Jul22-Dec22), C7 part I (Jan23-13Mar23) and C7 High fluence (14Mar23-12Apr23) campaigns. In terms of plasma exposure, the C6 campaign was not significant with a cumulated plasma duration of less than 5 min, we thus differentiated C5-C6, the first part of C7 and the second part of C7. The C5-C6 consist in cumulated duration of 1 h22 of D plasma exposure with 3 boronisations. The first part of C7 (~2h27 of D plasma exposure) was marked by a single boronisation after 1 h of D plasma exposure and was ended by an impact of the runaway electron beam on the inner bumper equipped with boron nitride (BN) tiles. Then the second part of C7, high fluence campaign [5] (~3h of D plasma and 0 boronisation) was performed to investigate plasma-wall interactions, using repetitive shots to reach an ITER relevant fluence and an expected significant W erosion/migration and subsequent deposition. To sum up the story, the deposits collected underwent the first high-fluence campaign carried out in 2023 after being exposed to some plasma from the C5-C6 campaigns and the first C7 period.

Deposits were collected on two separate PFUs. Fig. 1 shows the location of these two PFUs with respect to the typical heat load on WEST divertor simulated by PFCflux code [8]. Due to the ripple modulation pattern, PFU10 is located in the OSP max area whereas PFU17 is located in the inner strike point (ISP) max area leading a heat flux in the ISP zone higher for PFU17(x1.6) than for PFU10[9]. On the High Field Side (HFS) in the ISP region around the MB15 (position of the SP during the high fluence plasma), the simulation takes into account the shaping of MB leading to a shadowed area for the leading edge (dark blue area on the right of MBs in Fig. 1).

Deposits were collected on the inner side (HFS) in the thick deposit area for MB7 to MB12 near the ISP zone which is dominated by erosion. Fig. 2 shows a schematic representation of the erosion/deposition pattern and the visual inspection after collection. For both PFU10 and PFU17: coloured thin film are found for MB1-3, brown deposits are found for MB4-5, dark deposits are found for MB6-7 whereas for MB8-12 the collected deposits were mainly bright. This visual aspect correlates well with that was observed after phase I of WEST on ITER-grade PFUs [11]. One can note that in the thick deposit area a toroidal contrast along the larger dimension of monoblock is observed for PFU10 and not for PFU17. In addition, a bright thin W film [12] which is peeling off is

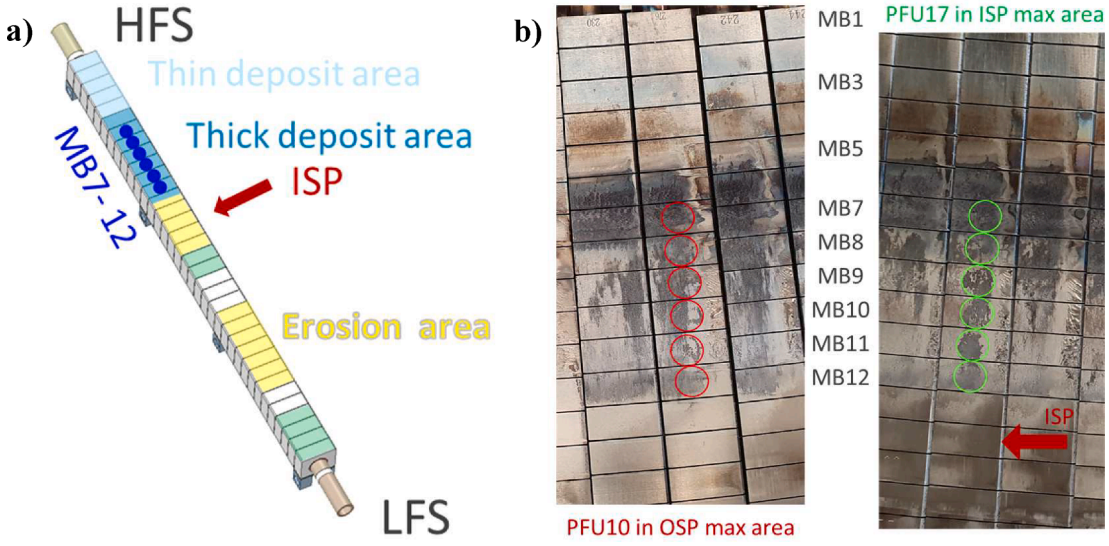

Fig. 2. View of the erosion/deposition pattern along the radial direction of PFUs: a) schematic representation with the location (blue dots) of the deposit collection presented here b) photographs for visual inspection of PFU10 and PFU17 after the high fluence campaign of WEST showing the fingerprint (coloured circles) of the deposit stamping collection. The "MB1…MB12" labels between the 2 photographs are marked for both PFUs.

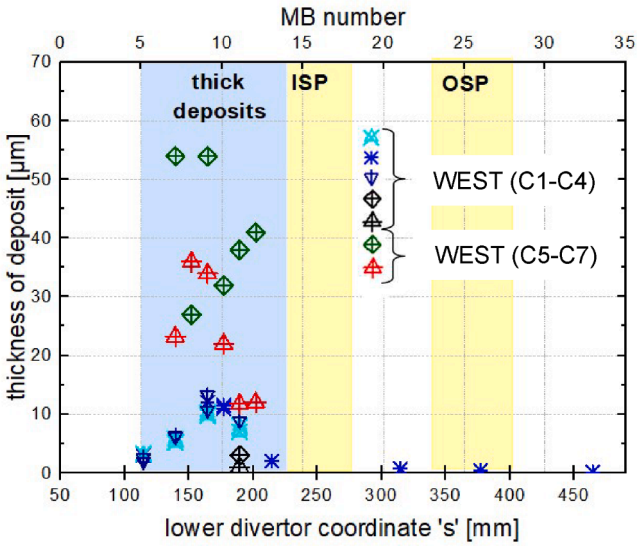

Fig. 3. Thickness of deposit along the radial direction for WEST (C1-C4) campaigns-cumulated plasma duration ~ 6 h- on ITER grade PFUs and for WEST (C5-C7) campaigns-cumulated plasma duration ~ 7 h- on ITER-grade PFU10 (red symbols) and on PFU17 (green symbols).

found on the leading edge. This toroidal deposition pattern at the monoblock scale is newly observed probably due to the combination of bevel, misalignment of PFU and to the detachment of the deposits. Deposits were sampled at the center of bevelled W MBs to disregard any toroidal deposition pattern on the MB.

Methods of collection and characterization

Deposits were collected in-situ during the WEST shutdown just after the high fluence campaign using the stamping procedure [13]. The sample holder with an adhesive carbon disk was manually pressed onto the monoblock, the fingerprint of the 12 mm diameter disk is highlighted in Fig. 2 by red and green circles. This method limits sample handling, PFUs cutting and was therefore used in-situ. However, it does not ensure that all deposits are collected, as adherent layers may be left on the PFU surface. It is therefore more relevant for thicker deposits which are less adherent, and enables a thickness to be measured which is probably underestimated. However, deposits caused by the end of the exposure history are analyzed with certainty, except only if they have flaked off during the last plasma exposures. A cross section of deposits stuck to the sample holder were cut by focused ion beam (FEI Helios 600 NanoLab) so that the whole deposit thickness and composition could be examined.

The cross section of deposits were analyzed using scanning electron microscopy (SEM, Zeiss Gemini SEM500) coupled with Energy Dispersive X-ray technique (EDX) using an EDAX SDD detector. Backscattered electron (BSE) images or secondary electron (SE) images were collected to highlight the chemical or topographic contrast. We performed EDX mapping on the cross section with a 5 kV incident energy and a high tilt of the sample (50-70°) optimizing the detection of light elements as B, C, O, N and minimizing the probed depth to compensate the tilt. Mappings of 512x400 pixels with 128 s per pixel enable the entire cross-section to be scanned for the thinnest deposits, and require the assembly of 2 or 3 mappings for the thickest deposits.

Morphology and composition of deposits

All the deposits show a multi-layer deposition structure, with layers of different morphology. The deposits composition is mainly W with B, O, C and N. A few Cu particles were observed in the layers but not presented, they were also present in the dust collected after the high-fluence campaign [12].

Thickness analysis along the radial direction

Fig. 3 displays the measured thickness in function of the s-coordinate of the lower divertor corresponding to the MB number. The red and green symbols are used to plot the thickness of deposits on PFU10 and PFU17, respectively. Thicknesses are found from 12 up to 55 µm for C5-C7 WEST.

The blue [10] and black [13] symbols represent thicknesses measured during the previous years on ITER-grade PFU3-7–11 and PFU10-17, respectively after the C1-C4 WEST campaigns using confocal microscopy or FIB cross section. Thicknesses were found from 3 up to 15 µm for C1-C4 WEST campaigns leading to a maximum campaign-averaged deposition rate of ~ 1.4 nm/s [10] which was in line with the results obtained for inertially cooled erosion marker components [14]. The sampling and measurement procedure used to obtain the black symbols is the one we used in this work, the thicknesses are underestimated compared to those in [10] as discussed in section 3.

In Fig. 3, the thickness evolution with s-coordinate for all measurement show maximum thicknesses are always obtained between MB8-10 with a more or less dome-like evolution. For PFU10 (red symbols) thickness shows a regular dome like evolution with a maximum for MB8 as previously observed over the C1-C4 period.

For PFU17 (green symbols) the maxima are observed for MB7 and MB9. One can note in addition that very high thicknesses are found near the ISP zone, up to 40 µm.

Despite roughly similar cumulative plasma durations (~6h for C1-C4 and ~ 7 h for C5-C7) and different sampling methods, deposit thicknesses are much higher (up to around 4 times higher) for C5-C7 than for C1-C4. The maximum campaign-averaged deposition rate was obtained of ~ 2.20 nm/s and of ~ 1.55 nm/s from the 55 µm thick layer on MB9PFU17 and the 38 µm thick layer on MB8PFU10, respectively. Analyzing the layers adhered to the carbon tape does not allow for a very accurate estimation of deposition rates, which are underestimated compared to the direct analysis of layers on the PFU. Nevertheless, despite this underestimation, these rates are still higher than the values reached during the phase I of WEST, clearly showing the high fluence campaign effect on deposition rate.

The tungsten deposition can be attributed to divertor sputtering/erosion of the neighboring inner strike point [15] and likely to the increased sources of tungsten impurities from other plasma facing components of WEST (upper divertor, baffle) as shown by the ERO2.0 simulations [16] while the contribution of tungsten from antenna limiters is negligible [15]. Off normal events contribution to the deposition must also be taken into account as they can produce not only dusts but also vapor of atomic W due to melting.

Thicknesses measured over the C1-C4 period on PFUs in different toroidal positions showed no significant difference, while thicker deposits are found for PFU17 compared to PFU10 for C5-C7 due to magnetic ripple modulation inducing highest flux on the ISP zone of PFU17 (strike point on MB16 during the high fluence campaign). The ripple effect measured on deposition seems to indicate that plasma discharges are clearly predominant in layer growth processes rather than transients or wall conditioning.

Structural analysis of the deposits

Fig. 4a) and Fig. 5a) show the morphology of the deposit cross sections over the C5-C7 campaign obtained for the MB7-12 on PFU10 and PFU17, respectively. The cross-sectional images are inverted to show the initial deposition at the bottom and the final deposition at the top. Thick and dense layers are found for the end of deposition for MB9-12 of both PFUs, they are highlighted by yellow arrows, while the layers underneath are thinner and more delaminated.

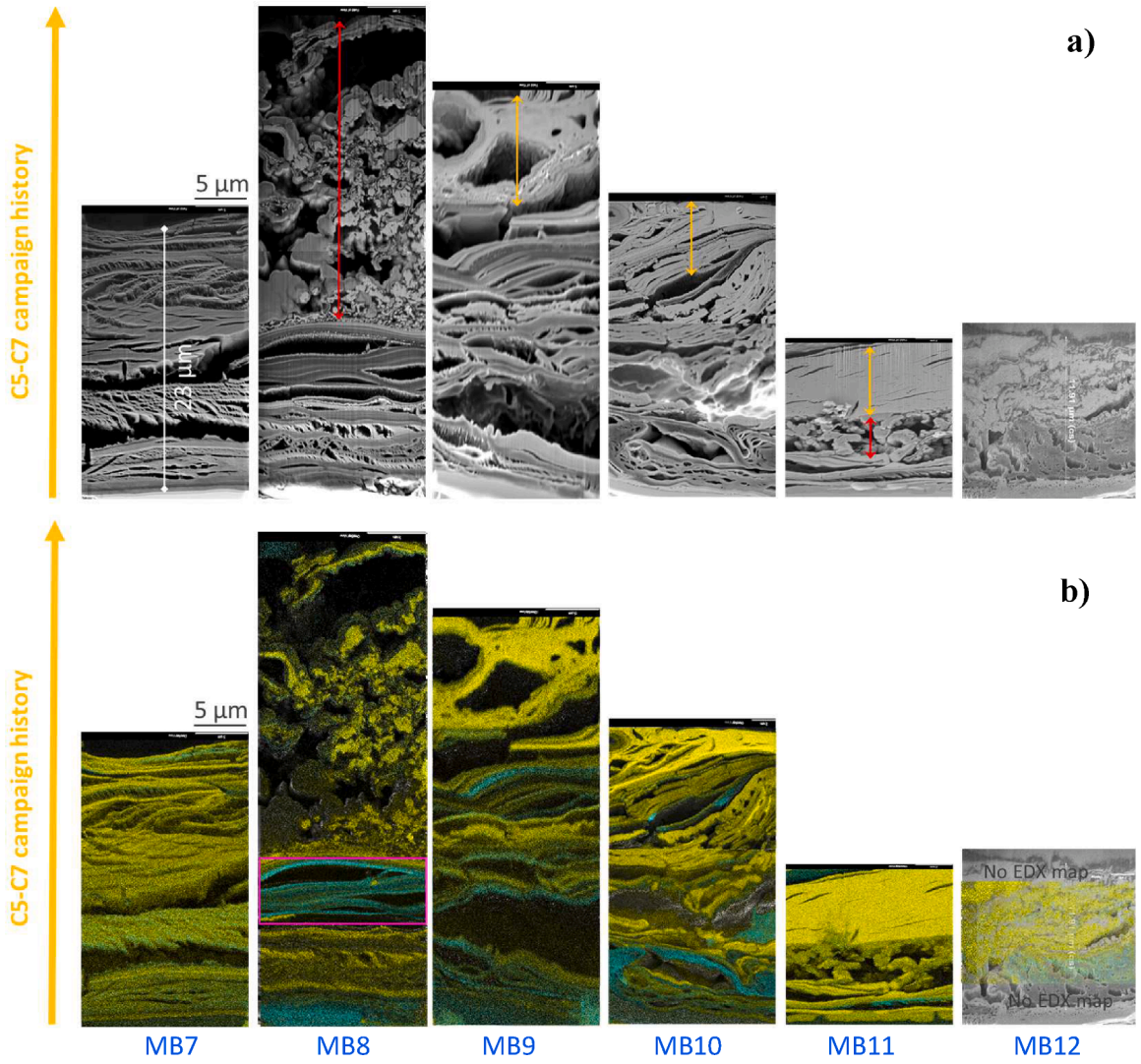

Fig. 4. Cross section of deposited layers on the PFU10 of the WEST lower divertor over the C5-C7 campaign history. Thick deposition area displayed from the HFS (left) to the ISP zone (right) along the radial direction from MB7 to MB12 **a)** SEM images showing the layer by layer structure deposition **b)** EDX mapping of deposited layers for W (yellow overlay) and B (turquoise overlay). All images are displayed at the same scale, the Y-axis scale is indicated by the white line while the X-axis scale is indicated by the black line. Yellow arrows highlight thick and dense layers of pure tungsten, red arrows highlight the melted area, and the pink frame shows the B + N-rich layer.

Porosities within the layers or porosities due to delamination of layers (10 % maximum of the total thickness) are observed in dark contrast. Thick and dense layers could exhibit large porosities of few µm for MB9 of PFU10 and MB9-12 of PF17. Thinner layers may exhibit a porous structure and greater delamination. The delamination may have been caused by oxidation of interface layers during plasma operation or baking due to combination of T≫Tamb and oxygen traces. Nevertheless, they may have also more likely been caused to air exposure after the vessel venting.

Melted parts, round-shaped aggregations of material with interconnected porosity, are found in deposited layers, they are highlighted by red arrows. They may have been caused by transients as disruptions or runaways electrons impacting the lower divertor. Indeed off-normal events could induce highly localized surface heating capable of melting the deposited layers, which then exhibit globular and porous structures after cooling. Some cracked layers have been observed on PFU17 reflecting the stress induced in deposited layer by the thermal cycling, the deposits can reach a surface temperature ranging from 100 to 400 °C according to the thermal analysis [6].

Fig. 4b) and Fig. 5b) show the tungsten and boron composition of the deposit cross sections over the C5-C7 campaign history obtained for the MB7-12 on PFU10 and PFU17, respectively. The EDX overlay of the mapped area is displayed in yellow for W and in turquoise for B. Basically, a bright yellow layer is pure tungsten and an intense turquoise layer is pure boron. The yellow arrows indicate deposits that do not contain B and consist only of pure W, as determined by a detailed EDX mapping analysis. Moreover, these deposits generally correspond to layers with lower porosity. The end of the deposition is marked by the black contrast on the top (Fig. 4.a and Fig. 5.a) caused by the carbon tape used in the stamping procedure. Note that for some areas corresponding to the yellow arrows of Fig. 4a) and Fig. 5a), a less intense yellow still corresponds to pure tungsten, due to the loss of X-ray signal caused by the sample inclination and shadowing effects. The oxygen was found everywhere except in the thick and dense layers found for the end of deposition for MB9-12 of both PFUs and highlighted by yellow arrows.

For the MB12 Fig. 4b) and MB11 Fig. 5b), the entire cross-section was deliberately not mapped, as the composition showed no variation. We found pure W for the top of the cross sections and B-rich for the bottom of the cross section of MB12 Fig. 4b). Elsewhere the area which are still gray not covered by the tungsten and boron overlays are

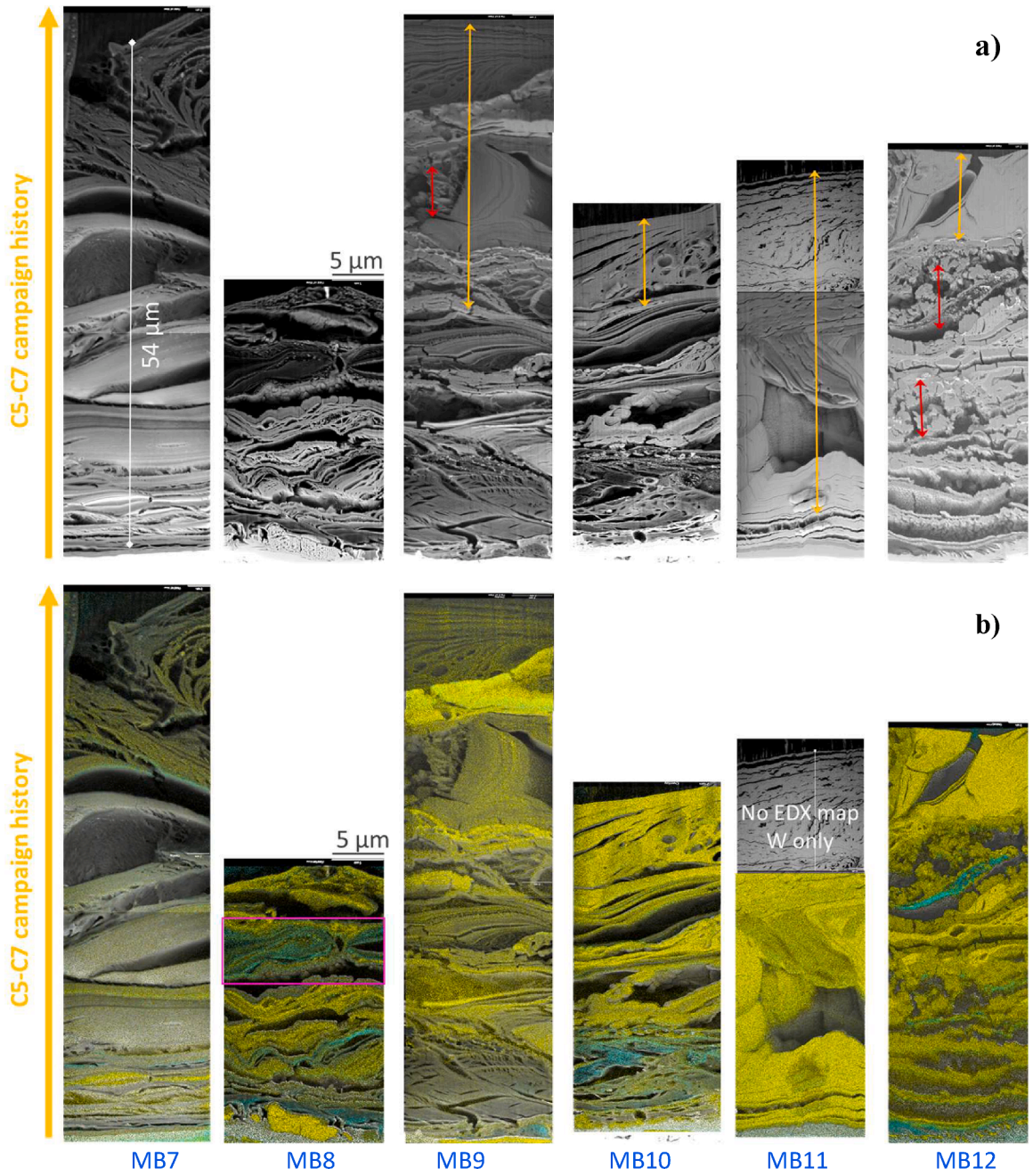

Fig. 5. Cross section of deposited layers on the PFU17 of the WEST lower divertor over the C5-C7 campaign history. Thick deposition area displayed from the HFS (left) to the ISP zone (right) along the radial direction from MB7 to MB12 **a)** SEM images showing the layer by layer structure deposition **b)** EDX mapping of deposited layers for W (yellow overlay) and B (turquoise overlay). All images are displayed at the same scale, the Y-axis scale is indicated by the white line while the X-axis scale is indicated by the black line. Yellow arrows highlight thick and dense layers of pure tungsten, red arrows highlight the melted area, and the pink frame shows the B + N-rich layer.

composed of C and O.

The common feature for both PFUs that we extracted from the composition analysis thanks to EDX mapping are the following:

- for MB9-12 (i) W-pure layers for the end of deposition that we attributed to the high fluence campaign effect (ii) B-rich layers in deposits mainly at the beginning of the deposition history attributed to the various boronisations during C5-C7 campaigns, the last one should mark the start of the high fluence campaign.
- for MB8 the EDX mapping analysis revealed a B + N-rich layer which is highlighted by pink frame in Fig. 4b) and 5b). They can be attributed to the impact of the runaway electron beam on the inner bumper equipped with BN tiles which occurred before the high fluence campaign.
- for MB7, no pure W or B layers are found, the deposit has a multilayer structure where W, B, O, C are mixed in all layers.

Finally, the deposits on MB8 of PFU17 which exhibit an unexpected low thickness and a deposition more or less ended by the B + N-rich layer produced before the high fluence has clearly revealed to be not complete. The layer deposited during the high-fluence campaign was probably lost during the campaign. This may have been the origin of an UFO, which is consistent with the observation of UFOs in the area of thick deposits in the maximum inner heat load area [6].

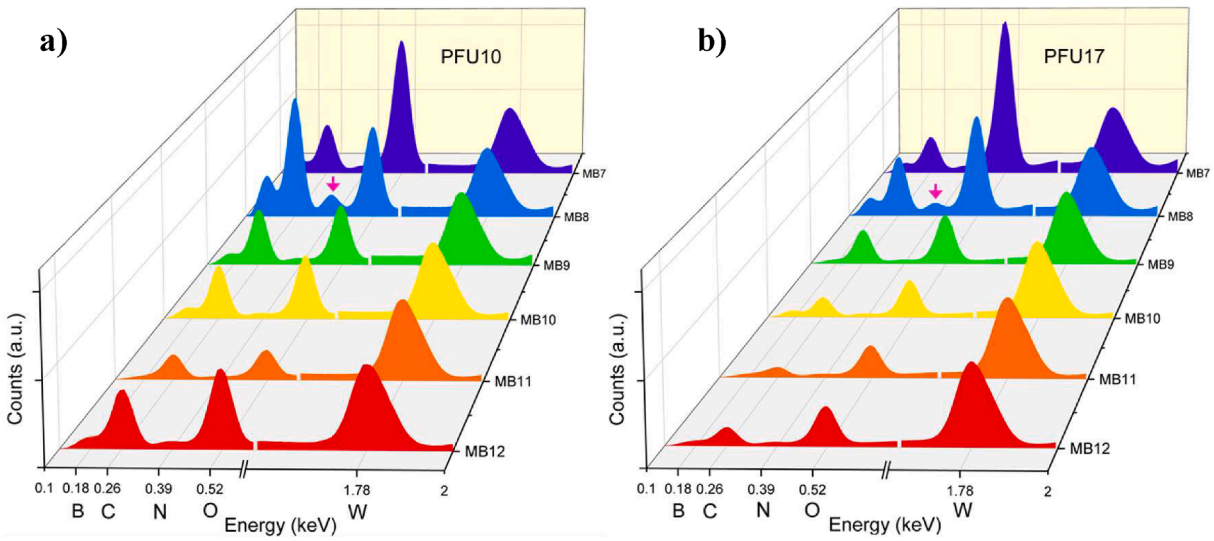

Fig. 6. Sum spectra of EDX mapping area of thick deposit cross-sections normalized by the W peak intensity for MB12 (red) to MB7 (dark blue) **a)** PFU10 located in the max OSP area **b)** PFU17 located in the max ISP area.

Composition analysis along the radial direction

In order to analyse the evolution of light elements B, C and O versus the W content along the radial direction of the WEST lower divertor, we used the sum spectrum of the EDX mapping area of the cross section. Fig. 6 displays the peak intensity evolution of B, C, O compared to the W peak which has been normalized for the spectra of MBs analysed on PFU10 and PFU17. For both PFUs the W content dominates in the deposits composition near the ISP area (MB12 to MB9) due to pure dense W layers of the high fluence campaign. Whereas the B and C contents are maximum on MB8 in agreement with the similar evolution observed using RBS/NRA [10] during the phase I of WEST. The deposition of light elements is dominant far in the scrape-off layer, while the deposition of tungsten is dominant very close to the erosion zone. This trend had already been observed in the deposition analyses after C3 and C4 campaigns [13] and seems to be confirmed here. A significant N peak (pink arrow in Fig. 6) is observed on MB8 corresponding to the B + N-rich layer (pink frame in Fig. 4b and 5b)). One can note that the O content is relatively very high for MB7 where the deposits are dark and mixed all elements. Although this effect is observed on both PFUs, the origin of the oxygen, which may come from intense post-mortem oxidation due to the structure and composition of the layers, or from in-situ deposition, is still unclear.

Conclusion

Deposits formed on the inner side of the lower divertor were analyzed for morphology and composition after the high fluence campaign in WEST in 2023. Deposits collected on ITER-grade PFUs were found to be very thick (12–55 μm) and composed mainly of W co-deposited with B, C, O and N, the maximum thickness was obtained for MB9 corresponding to an s-coordinate of 150 mm in the radial direction, which corresponds well with an earlier post-mortem studies after phase I of WEST [10]. The difference lies in the observation of thick deposits of up to 40 μm in the area MB9-12 near ISP, composed of an almost pure layer of tungsten with very little oxidation and carbon contamination. Analyzing the deposits collected on two PFUs in different toroidal position, thicker deposits (up to 55 μm) for the PFU located at the maximal heat load in the inner side and thinner deposits for the PFU located in low heat load in the inner side (up to 38 μm) were obtained leading to deposition rates of about 2.2 nm/s and 1.55 nm/s, respectively. Their ratio (x1.44) correlates well to the heat load ratio (x1.6) due to the toroidal magnetic field modulation. The delaminated and/or porous structures and the pure tungsten composition of the thick deposits near the erosion zone on the inner side are favorable for the UFO formation observed during the high fluence campaign.

CRediT authorship contribution statement

C. Martin: Writing – review & editing, Writing – original draft, Methodology, Investigation, Funding acquisition, Formal analysis. **M. Diez:** Writing – review & editing, Validation, Funding acquisition. **E. Bernard:** Resources. **M. Cabié:** Investigation. **A. Campos:** Investigation. **C. Pardanaud:** Writing – review & editing. **G. Giacometti:** Investigation. **A. Gallo:** Writing – review & editing. **J. Gaspar:** Writing – review & editing, Formal analysis. **Y. Corre:** Formal analysis. **E.Tsitrone:** .

Declaration of competing interest

The authors declare that they have no known competing financial interests or personal relationships that could have appeared to influence the work reported in this paper.

Acknowledgments

This work has been carried out within the framework of the EUROfusion Consortium, funded by the European Union via the Euratom Research and Training Programme (Grant Agreement No 101052200 — EUROfusion). Views and opinions expressed are however those of the author(s) only and do not necessarily reflect those of the European Union or the European Commission. Neither the European Union nor the European Commission can be held responsible for them.

Data availability

No data was used for the research described in the article.

References

[1] J. Bucalossi, et al., Operating a full tungsten actively cooled tokamak: overview of WEST first phase of operation, Nucl. Fusion 62 (2022) 042007.
[2] M. Missirlian, et al., Manufacturing, testing and installation of the full tungsten actively cooled ITER-like divertor in the WEST tokamak, Fusion Eng. Des. 193 (2023) 113683, https://doi.org/10.1016/j.fusengdes.2023.113683.
[3] R.A. Pitts, et al., Physics conclusions in support of ITER W divertor monoblock shaping, Nuclear Materials and Energy 12 (2017) 60–74, https://doi.org/10.1016/j.nme.2017.03.005.

[4] M. Diez, et al., Experimental characterization of leading edge cracking on bulk tungsten divertor components during 2017-2019 WEST operation, Nuclear Materials and Energy 41 (2024) 101745.
[5] R.A. Pitts, et al., Physics basis for the first ITER tungsten divertor, Nuclear Materials and Energy 20 (2019) 100696, https://doi.org/10.1016/j.nme.2019.100696.
[6] J. Gaspar, et al., Thermal and statistical analysis of the high-Z tungsten-based UFOs observed during the deuterium high fluence campaign of the WEST tokamak, Nuclear Materials and Energy 41 (2024) 101745.
[7] A. Gallo, et al., Wall conditions in WEST during operations with a new ITER grade, actively cooled divertor, Nuclear Materials and Energy 41 (2024) 101741.
[8] M. Firdaouss, et al., Heat flux depositions on the WEST divertor and first wall components, Fusion Eng. Des. 98–99 (2015) 1294–1298.
[9] A. Grosjean, et al., First analysis of the misaligned leading edges of ITER-like plasma facing units using a very high resolution infrared camera in WEST, Nucl. Fusion 60 (2020) 106020.
[10] M. Diez, et al., Overview of plasma-tungsten surfaces interactions on the divertor test sector in WEST during the C3 and C4 campaigns, Nuclear Materials and Energy 34 (2023) 101399, https://doi.org/10.1016/j.nme.2023.101399.
[11] M. Diez, et al., Nucl. Fusion 61 (2021) 106011, https://doi.org/10.1088/1741-4326/ac1dc6.
[12] C. Arnas, et al., Dust collection after the high fluence campaign of the WEST tokamak, Nuclear Materials and Energy 41 (2024).
[13] C. Martin, et al., First post-mortem analysis of deposits collected on ITER-like components in WEST after the C3 and C4 campaigns, Phys, Scr. 96 (2021) 124035, https://doi.org/10.1088/1402-4896/ac267e.
[14] M. Balden, et al., Erosion and redeposition patterns on entire erosion marker tiles after exposure in the first operation phase of WEST, Phys. Scr. 96 (2021) 124020, https://doi.org/10.1088/1402-4896/ac2182.
[15] N. Fedorczak, et al., Tungsten gross erosion from main plasma facing components of WEST during a L-mode high fluence campaign, and its relation to the formation of divertor deposits, Nuclear Materials and Energy 41 (2024) 101758.
[16] G. Ciraolo, et al., 3D SOLEDGE-ERO2.0 simulations for tungsten sources and migration in WEST discharges and comparison with experimental data, Nuclear Materials and Energy 41 (2024).